



Published in final edited form as:

Anal Chem. 2010 May 1; 82(9): 3707–3713. doi:10.1021/ac100042e.

## Fluorescent Nano-Optodes for Glucose Detection

Kelvin Billingsley<sup>†,1</sup>, Mary K. Balaconis<sup>†</sup>, J. Matthew Dubach<sup>†</sup>, Ning Zhang<sup>‡</sup>, Ed Lim<sup>‡</sup>, Kevin P. Francis<sup>‡</sup>, and Heather A. Clark<sup>†,\*</sup>

<sup>†</sup>The Charles Stark Draper Laboratory, Bioengineering Group, 555 Technology Square, Cambridge, MA 02139, USA.

<sup>‡</sup>Caliper Life Science, 2061 Challenger Drive, Alameda, CA 94501 USA.

### Abstract

We have designed fluorescent nanosensors based on ion-selective optodes capable of detecting small molecules. By localizing the sensor components in a hydrophobic core, these nanosensors are able to monitor dynamic changes in concentration of the model analyte, glucose. The nanosensors demonstrated this response *in vitro* and also when injected subcutaneously into mice. The response of the nanosensors tracked changes in blood glucose levels *in vivo* that were comparable to measurements taken using a glucometer. The development of these nanosensors offers an alternative, minimally-invasive tool for monitoring glucose levels in such fields as diabetes research. Furthermore, the extension of the ion-selective optode sensor platform to small molecule detection will allow for enhanced monitoring of physiological processes.

---

The introduction of fluorescent nanosensors, or PEBBLEs, made possible the intracellular analysis of a range of analytes which was previously impractical with molecular indicators. Based on ion-selective optode technology, nanoscale PEBBLEs were produced that could measure a large host of physiological parameters, including sodium, potassium and chloride.<sup>1–6</sup> Further refinements of the sensors led to better stability and biocompatibility necessary for intracellular measurements.<sup>7</sup>

Extending this nanosensor approach beyond detection of ions to small molecules has several limitations. Recognition elements for small molecules are traditionally based on biological reagents, such as enzymes (*e.g.* glucose oxidase<sup>8, 9</sup> or urease<sup>10</sup>) or non-enzymatic proteins (*e.g.* antibodies or Concanavalin A<sup>11</sup>). Although these sensors function adequately when applied on large length scales, when the size of these sensors is radically scaled down, shortened lifetimes can occur due to regional depletion of resources, such as oxygen in the case of glucose oxidase function.<sup>8, 9</sup> In addition, since a limited number of biological elements are contained in the small sensor volume employed, any degradation greatly diminishes the function of the sensor.

When encapsulating an enzyme, the choices of polymeric shells are limited to hydrophilic components, such as hydrogels, in order to maintain function. As shown with ion-selective optodes, though, there are several advantages to using a lipophilic system for nanosensor development. First, it greatly expands the range of measurable analytes by enabling the use of a wider variety of chemistries. Second, by separating all of the lipophilic molecular components in the nanosensors from the bulk, aqueous solution, non-specific binding to proteins can be

---

\*Correspondence: Heather A. Clark, Ph.D., hclark@draper.com.

<sup>1</sup>Kelvin Billingsley, Ph.D., Stanford University, Chemistry Department, 333 Campus Drive, Stanford, CA 94305-5080

SUPPORTING INFORMATION AVAILABLE

Additional information as noted in text. This material is available free of charge via the Internet at <http://pubs.acs.org>.

reduced.<sup>4</sup> Third, the lipophilic core maintains these components at the proper concentrations leading to improved lifetime and stability of the nanosensors.<sup>7</sup> Fourth, keeping the component in close proximity allows a completely reversible response of the nanosensors to dynamic changes in ion or small molecule concentration. Finally, the lipophilic environment makes possible an easily functionalized and tunable system. By adjusting the concentration of molecular components, the nanosensors can be tuned to respond within the ideal dynamic range and due to the ease of adding biocompatible surface coatings, these nanosensors can be made compatible with an intracellular environment and experience minimal aggregation.<sup>7, 12</sup>

Building on this lipophilic nanoscale platform, we introduce the first example of this class of optode-based nanosensor for small molecule recognition utilizing non-biological components. As a model analyte we demonstrate the detection of glucose. The nanosensor responds to glucose through the use of lipophilic boronic acid (BA) derivatives which have been extensively characterized as glucose recognition molecules.<sup>13, 14</sup> Other researchers have exploited the affinity of BA for glucose to design a variety of glucose sensors. Asher *et al.*, for example, have developed photonic crystals that swell in the presence of glucose.<sup>15–17</sup> Through measuring the light diffraction properties of the crystal, the glucose concentration can be inferred. Our chemistry, however, relies on a competitive binding mechanism between a lipophilic BA and a chromophore, alizarin.<sup>18, 19</sup> Glucose is reversibly extracted into the sensor by a BA in a similar fashion as previously reported for ion-based sensors.<sup>7</sup> As depicted in Scheme 1, alizarin, a non-fluorescent compound, reacts with a BA to produce a boronate ester, **1**. Importantly, **1** is highly fluorescent and favored in the chemical equilibrium; therefore, the dissociation of **1** can be monitored by the loss of fluorescence intensity. When glucose is introduced into the equilibrium, a shift from the fluorescent species, **1**, to glucose-derived boronate ester, **2**, and non-fluorescent alizarin is observed. Therefore, the change in fluorescence intensity corresponds to the glucose concentration. A similar scheme has been used by James and Fossey to detect glucose using a solution phase assay and hydrogels, respectively.<sup>19, 20</sup> However, as previously mentioned, our system entraps the sensor components within the lipophilic core maintaining these components at the ideal sensing ratio.

Glucose plays a critical role in the body's metabolism and dysfunction of glucose handling from insulin deficiency or resistance can lead to diabetes. Thus, the detection and monitoring of glucose has been the focus of diabetes-related research and technology. For this reason, glucose was chosen as the model analyte for our nanosensor because of the applicability of the nanosensors as both a research and diagnostic tool.

## EXPERIMENTAL SECTION

### Materials

Poly(vinylchloride) carboxylated (>97% GC), *bis*-(2-ethylhexyl)sebacate, tridodecylmethylammonium chloride and alizarin were purchased from Fluka (St Louis, MO, USA). *D*-(+)-glucose (ACS reagent grade), uric acid (≥ 99%, crystalline), acetaminophen (≥ 99%) and *L*-ascorbic acid (≥ 99%, crystalline) were obtained from Aldrich Chemical Co (St Louis, MO, USA). Octylboronic acid (>97%) and 1,2-distearoyl-*sn*-glycero-3-phosphoethanolamine-N-[methoxy(polyethylene glycol)-550] (PEG lipid) in chloroform (10 mg/ml) were acquired from Synthonix (Wake Forest, NC, USA) and Avanti Polar Lipids, Inc. (Alabaster, AL, USA), respectively. Phosphate Buffered Saline (PBS) (1×, pH = 7.4) was purchased as a solution from Invitrogen (Carlsbad, CA, USA). Tetrahydrofuran (≥ 99%) (THF) was acquired from Sigma (St Louis, MO, USA). Chloroform (HPLC grade) was purchased from JT Baker (Phillipsburg, NJ, USA). Commercially available materials were used without further purification. CD1 mice were obtained from Charles River Laboratories International, Inc (Wilmington, MA, USA) and weighed 20–25 g.

### Polymer Composition of the Optode

The polymer optode was made from the following components: 30 mg high molecular weight carboxylated poly(vinylchloride), 60  $\mu$ l *bis*-(2-ethylhexyl)sebacate, 3.0 mg octylboronic acid, 4.0 mg tridodecylmethylammonium chloride, and 1.0 mg alizarin. These materials were charged into a glass vial and then dissolved in 500  $\mu$ l THF. The vial was vortexed and the resulting optode was an orange solution.

### Calibration of the Macrosensor

Data was acquired in a Spectramax Gemini EM microplate fluorometer (Molecular Devices, Sunnyvale, CA, USA). Optode (2  $\mu$ l) from a bulk batch containing four times each of the components listed above was pipetted into 33 wells of a 96-well optical bottom plate each containing a glass cover slip. The optodes were then allowed to dry at least 15 minutes forming macrosensors. Each optode was hydrated in 200  $\mu$ L PBS (pH=7.4) for at least 4 hours until the fluorescence signal stabilized. At the end of this period, the PBS solution was removed and another 200  $\mu$ L of fresh PBS was added to the wells. After 40 minutes, an endpoint measurement was collected via exciting at 460 nm and emitting at 570 nm with a cutoff of 515 nm. The PBS solution was then replaced with 200  $\mu$ l of 1 mM glucose in PBS (pH = 7.4). The optodes were allowed to equilibrate for 40 minutes, followed by an endpoint measurement. The process was repeated for 2 mM, 3 mM, 5 mM, 8 mM, 10 mM, 25 mM, 50 mM, 100 mM, 500 mM, and 1 M glucose in PBS. Response was determined by expressing the data as  $\alpha = (I_{\max} - I)/(I_{\max} - I_{\min})$ .  $I$  is the intensity at the given glucose concentration,  $I_{\min}$  is the intensity at the minimum signal, and  $I_{\max}$  is the intensity at the maximum signal. A sigmoidal curve was fitted to the plot of  $\alpha$  vs. log [glucose concentration] Molar using Origin software (Northampton, MA, USA). The  $K_d$ , center of the dynamic range, was determined as the glucose concentration where  $\alpha$  is equal to 0.5 on the calibration curve. Furthermore, the sensitivity of the sensors was calculated from the slope of the linear region of the sigmoidal curve.

### Reversibility of the Macrosensor

Macrosensors of a single optode batch were prepared by the procedure described above using 16 wells. After the optodes were hydrated, the PBS solution was removed from all wells and 200  $\mu$ l of 1 M glucose in PBS was pipetted into 8 wells. The remaining 8 wells acted as controls and contained fresh glucose-free PBS. In order to track the changes in the fluorescence response, measurements were acquired at a sampling rate of 5 minutes for 60 minutes. Then, all solutions (glucose and control) were removed and 200  $\mu$ l of fresh PBS was added to all wells. Again, measurements were obtained every 5 minutes for 60 minutes. An additional cycle was performed to yield a total experiment time of 4 hours. Response was determined by the percent change difference between the average intensity of the glucose and control. Figure 1C was generated by averaging the fluorescence intensity of the individual macrosensors for the three time points prior to a solution change. These values were then standardized and the percent change was calculated as the difference between the average standardized intensity of the glucose and control. The error was generated from the raw intensity values using the laws of error propagation.

### Effects of Interferents

Calibration of the macrosensors was performed as described above with PBS and glucose solutions that contained either no interferent, uric acid (20 mg/dl), ascorbic acid (3 mg/dl) or acetaminophen (20 mg/dl).<sup>21</sup> The glucose concentrations used in the calibration were 0 mM, 1 mM, 3 mM, 5 mM, 10 mM, 25 mM, 50 mM, 100 mM, and 1M. Response was compared by fitting a sigmoidal curve to the plot of  $\alpha$  vs. log [glucose concentration] Molar for each interferent using Origin software.

## Nanosensor Fabrication

The optode was allowed to dry on a glass surface for at least 4 hours. The optode film was removed and transferred to a glass vial. The vial was then charged with 5 ml of PBS and 5 mg of surface modifier, 1,2-distearoyl-*sn*-Glycero-3-Phosphoethanolamine-N-[Methoxy (Polyethyleneglycol)-550] (PEG lipid), in 0.5 ml chloroform. This solution was sonicated with a probe-tip sonicator (Branson, Danbury, CT, USA) at 40% amplitude for 3 minutes. The residual polymer was discarded to yield the nanosensor solution.

## Particle Sizing and Zeta Potential

Particle size and zeta potential of the nanosensors were determined using a nanosizer (Nano Series ZS90, Malvern, Worcestershire, UK). Data was acquired for nanosensors made on five different days. A minimum of five runs was performed for each fabrication. The average and standard deviation of measurements were then calculated ( $n = 31$ ). The reported size is the Z-Average or the “cumulants mean” which is an intensity mean of the nanosensors.<sup>22</sup>

## Spectrum of Nanosensors

Data was acquired in a Spectramax Gemini EM microplate fluorometer (Molecular Devices) by exciting at 460 nm and scanning the emission from 510–690 nm. 100  $\mu$ l of nanosensors in PBS was pipetted into 8 wells of a 96-well optical bottom plate. Glucose in PBS was added to each well to bring final concentrations to 0 mM, 0.5 mM, 5 mM, 15.8 mM, 50 mM, 158 mM, 0.5 M or 1 M. This process was repeated in quadruplicate for each glucose concentration with each well having equivalent volume.

## Calibration of Nanosensors

Data was acquired in a Spectramax Gemini EM microplate fluorometer exciting at 460 nm and emitting at 570 nm with a cutoff of 515 nm. 60  $\mu$ l of nanosensors in PBS was pipetted into 12 wells of a 96-well optical bottom plate. Glucose in PBS was added to each well to bring final concentrations to 0 mM, 0.5 mM, 1 mM, 1.5 mM, 2.5 mM, 4 mM, 5 mM, 12.5 mM, 25 mM, 50 mM, 250 mM, and 500 mM glucose. This process was repeated in quadruplicate for four sets of glucose nanosensors at each glucose concentration with each well having equivalent volume. This process was repeated at 4 and 8 hours after sensor fabrication in order to determine the lifetime of the sensors. Response was determined by expressing the data as  $\alpha = (I_{\max} - I) / (I_{\max} - I_{\min})$ . The error for  $\alpha$  was calculated from the raw fluorescence intensity values using the laws of error propagation. A sigmoidal curve was fitted to the plot of  $\alpha$  vs. log [glucose concentration] Molar using Origin software.

## Leaching of Nanosensors

Data was acquired in a Spectramax M2 fluorometer (Molecular Devices) exciting at 460 nm and emitting at 570 nm with a cutoff of 515 nm. 500  $\mu$ l of nanosensors in PBS mixed with an additional 500  $\mu$ L of PBS was placed in a cuvette. The intensity of the nanosensors was tracked every 10 minutes for approximately 17 hours. The intensity was normalized to its initial value in order to get the percent change over time.

## Photobleaching of Nanosensors

Optical data was collected on an IVIS® 200 (Caliper, Hopkington, MA, USA) *in vivo* animal imager with both excitation and emission filters set to GFP. Three 1  $\mu$ l spots of nanosensors were placed on a glass microscope slide and imaged every 2 minutes for 94 minutes. The average efficiency for each spot was standardized to the time after the spots had dried. The standardized average efficiency was tracked over time in order to determine the effects of photobleaching.

## **In Vivo Studies**

Optical data was collected with the IVIS® Spectrum (Caliper, Hopkington, MA, USA) *in vivo* animal imager. Each mouse was shaved and then fasted for 18 hours. Four mice (two glucose and two controls) were employed in each experimental run. Mice were anesthetized with 3% isoflurane in oxygen. Blood glucose measurements from the tail of each mouse were taken with a LifeScan OneTouch® Ultra® (Langhorne, PA, USA) glucose meter and corresponding test strips prior to injection of the nanosensors. Then, 10  $\mu$ l of the nanosensors were injected into the subcutaneous region at four locations along each of their backs. All four mice were simultaneously imaged every 2 minutes for 15 minutes. Excitation and emission wavelengths were chosen as 500 and 600 nm, respectively, based on the available filter sets on the IVIS® Spectrum. At this point, a second blood measurement was taken with the glucometer prior to oral gavage. Then, the two control mice were administered an oral gavage of 300  $\mu$ l saline, and the two glucose mice were administered 300  $\mu$ l of saline containing glucose (3 g/kg). Glucose administration through oral gavage has been shown in previous mice studies to produce a systemic rise in blood glucose levels<sup>23</sup> and was covered under the approved animal protocol. All four mice were simultaneously imaged every 2 minutes for 10 minutes. Then, another blood measurement was taken with the glucometer. The same cycle of imaging followed by blood glucose measurement was repeated until a total of 6 cycles had been performed. This process was repeated to obtain an n = 4 for both the control and glucose.

At the point of oral gavage, the percent change of optical intensity was set to 0%. Any loss of optical intensity detected in the control mice was determined to be diffusion of the nanosensors away from the point of injection. The optical data collected from each glucose mouse was normalized versus the control mice signal in order to accurately estimate the percent change attributable to glucose and account for the effect of diffusion on signal loss. A plot of the percent optical change and blood glucose measurements versus time for each mouse is shown in Figure S-2.

In order to correlate the percent optical change from the nanosensors with blood glucose measurements, the average percent intensity change was determined for each blood glucose reading by averaging the two optical intensities closest to the reading. The percent optical change before and after blood readings was averaged for measurements obtained during the experiment. The initial and end blood measurements were correlated to the two points after and before blood readings, respectively. A line was fitted to the xy-scatter plot of percent optical change data points vs. glucose concentration for each mouse using Origin software. The fitted line provided a calibration between the optical response of the nanosensors and the blood glucose concentration for each mouse. In order to compare the calibrations among the experiments, the glucose concentration for each optical data point was determined from the equation of the fitted line for each mouse. An xy-scatter plot of the glucose concentration from the optical data vs. measured blood glucose readings for all mice is shown in Figure 3C. A line was fitted to this plot using Origin software. The correlation coefficient from this plot describes the variability among these data points and the four calibrations.

## **RESULTS AND DISCUSSION**

### **Macrosensor Development**

The development of the glucose-sensitive nanosensors first begins on the macro-scale so that the optimal sensor formulation is determined prior to nanosensor fabrication. The sensor matrix consists of plasticized poly(vinylchloride) carboxylate, octylboronic acid, alizarin and the ionic additive, tridodecylmethylammonium chloride. The sensor components are dissolved in THF creating an optode. Through optimization of these molecular components and their respective ratios, an optical macrosensor was developed to respond to glucose in the physiological range

(1–25 mM).<sup>24</sup> As depicted in Figure 1A, the fluorescence response of the macrosensor was measured from low (1 mM) to high (1 M) levels of glucose. The dissociation constant ( $K_d$ ) for the macrosensor was determined to be 19 mM by sigmoidal curve fit analysis. The linear region of the curve encompasses the physiological range where the sensors have a sensitivity of 0.2 mM per percent change of fluorescence intensity. We also measured macrosensor response to glucose in the presence of common interferents of electrochemical reactions that produce falsely high readings for numerous enzyme-based sensors.<sup>21</sup> These compounds, uric acid, ascorbic acid and acetaminophen did not result in statistically significant differences in the response (Figure 1B). Boronic acids are known to bind to diols such as nucleotides and saccharides<sup>13, 14, 25</sup>, but the interference of other sugars such as fructose and galactose was not measured because of their low concentration (<1 mM<sup>26</sup>) found at physiological conditions which is below the dynamic range of our sensor formulation. Furthermore, we assessed the macrosensor response from pH 6.8 to 7.8 due to its physiological relevance (blood pH=7.427) and found no statistical difference in response within this range ( $p > 0.05$ , data not shown). The macrosensor response would be expected to shift at more acidic and basic pHs due to alizarin's pKas at 6.2 and 11.128; however, this pH range was not analyzed since these values fall outside the relevant physiological range. In addition, the response of the macrosensor to glucose proved to be reversible (Figure 1C). This cycle of response and recovery could be repeated multiple times with only slight loss of response. Due to the size of the macrosensor, the response was measured over one hour. This response time is approximately 3 times longer than sodium macrosensors (data not shown). Miniaturizing the sodium sensors to the nanoscale reduces the estimated response time to microseconds.<sup>7</sup> Thus miniaturizing the glucose macrosensors to the nanoscale should result in a response time on the order of at least seconds which would be acceptable for a monitoring device.

### Nanosensor Development

Nanosensors were constructed through rigorous sonication of a mixture containing dried optode, PBS, and PEG-lipid surface modifier dissolved in chloroform. The modifier is an amphiphilic molecule that readily inserts into the hydrophobic sensor, leaving the hydrophilic, biocompatible component on the outside of the nanosensor exposed to the aqueous environment. This coating stabilizes the nanosensors in solution and imparts biocompatibility.<sup>7</sup> The average size of the nanosensors was  $74.2 \text{ nm} \pm 39.8 \text{ nm}$ , as measured with a Nano Series ZS90 particle sizer (Malvern, Worcestershire, UK).

The response of the nanosensors to glucose was initially examined in a well plate, and a wide dynamic range was observed (Figure 2). As can be seen, even at high concentrations of glucose, saturation of the signal was not possible. The sensors had a measured  $K_d$  and sensitivity of 38 mM and 2 mM, respectively. The nanosensors still responded within the physiological range, but suffered some loss of sensitivity due to the miniaturization process. The response of the nanosensors to glucose was also monitored over time. Minimum differences were observed between the 0 hour and 4 hour calibrations, but a slight shift in nanosensor response was seen after 8 hours (Figure 2). The slight shift in response could be due to the gradual leaching of sensor components caused by the increased surface area to volume ratio of the sensors.

### *In Vivo* Response of Nanosensors

The glucose-sensitive nanosensors were evaluated *in vivo* by tracking the qualitative changes in blood glucose levels, measured with a glucometer, against the optical response of the nanosensors. Mice were anesthetized then injected subcutaneously with nanosensors in PBS along the back (Figure 3A). Images were taken for 15 minutes to establish a baseline fluorescence intensity. During this time, a decrease in fluorescence intensity was observed, which was attributed to the equilibration of the sensors with the resting glucose levels of the mice and sensor diffusion away from the injection site. Though we could not quantifiably

monitor fluorescence staining due to the optical resolution of the instrument, we believe that the sensors diffused into the blood stream. To account for sensor diffusion away from the point of injection, all mice were paired with controls (no oral glucose). Blood glucose measurements were taken from the tail vein and analyzed with a LifeScan OneTouch® Ultra® glucometer. The LifeScan OneTouch® Ultra® glucometer has been FDA-approved for measuring glucose levels in diabetic care.<sup>29</sup> After baseline was established, mice were given an oral gavage of either saline (control) or glucose solution. This method of administering glucose has been shown effective for increasing blood glucose levels in mice.<sup>23</sup> Optical measurements were subsequently taken every 2 minutes for a 10 minute span followed by a blood glucose reading. This cycle of optical and blood measurements was conducted for one hour after glucose gavage.

Figure 3B displays the optical response and blood measurements for an individual mouse over the course of an experiment. The sensor response correlated with blood glucose readings, and this relationship was maintained over the course of analysis. Both monitoring methods initially detected a significant increase in glycemic levels due to the glucose gavage. The glucose levels eventually stabilized, presumably as the mouse produced an endogenous insulin response to the elevated glucose levels. The nanosensors demonstrated a rapid response to variations in glycemic levels, which is an inherent feature of the chemical equilibrium established in our sensor design. This attribute of the nanosensors allowed for a more continuous glucose analysis than the single-point measurements. The nanosensors tracked blood glucose concentrations from 66 mg/dl, 3.7 mM, to 427 mg/dl, 23.7 mM. The large error bars for the optical response could be due to the injection technique and biological variation such as the metabolic rate for each mouse. No error bars are present for the blood glucose measurements as only one blood sample was taken each sequence because of blood volume limitations in mice.<sup>30</sup> The correlation between optical response and blood measurements was consistent for each mouse examined in the study (Figure S-2). Although the upper detection limit of the blood glucose monitor is 600 mg/dl, higher glycemic levels are capable of being optically detected as shown in Figure 2.

The *in vivo* measurements for all mice were correlated to confirm the relationship between optical response and blood glucose concentration in each experiment. The average percent intensity change was determined for each blood glucose reading. For each mouse, a linear relationship between optical and blood glucose was obtained (data not shown). The calibration for each mouse was then used to determine the calculated glucose concentration from the optical data at the time of each blood measurement. Figure 3C displays the xy-scatter plot of these data points for all mice. The linear fit of the data indicates that optical measurements correlated to blood glucose measurements over the entire range of glucose concentrations when the data from all animals is combined. Throughout the *in vivo* experiments, glycemic levels were found to vary between 66 mg/dl, 3.7 mM, and 537 mg/dl, 29.8 mM. The glucose concentrations obtained from the optical response of the glucose-sensitive nanosensors were consistent with the measurements acquired from the glucometer in this critical span. This correlation demonstrates that subcutaneous injections can reflect blood glucose levels and that nanosensor response is unaffected by the *in vivo* conditions. Literature is available regarding regional differences and time lags in glucose levels throughout the body<sup>31-34</sup>; however, accounting for these differences will be the focus of future work. In addition, the change in optical signal is not significantly attenuated by the skin of the mouse. Future work will include optimizing the sensor response within the hypoglycemic range, performing *in vivo* sensor calibration, and incorporating a reference dye into the sensors to minimize variation in sensor response due to injection techniques and inherent biological variation.

## CONCLUSION

In summary, we have designed glucose-sensitive nanosensors that exploit the competitive binding properties of aryl and alkyl diols with boronic acids. This chemistry is maintained within a hydrophobic core which limits effects of interferents and maintains, in close proximity, the components required for reversibility of the competitive binding. The nanosensors have not only demonstrated this reversible response to dynamic changes in glucose concentration, but they also have a dynamic range encompassing physiologically relevant glucose levels. Furthermore, the nanosensors tracked rapidly changing glucose concentrations *in vivo* which corresponded to blood glucose levels measured with a glucometer. The ability of the nanosensor system to monitor glucose dynamics *in vivo* could be applied to diabetes treatment as well as applications in research, such as monitoring the effects of  $\beta$ -cell function or novel treatments for the disease.

## Supplementary Material

Refer to Web version on PubMed Central for supplementary material.

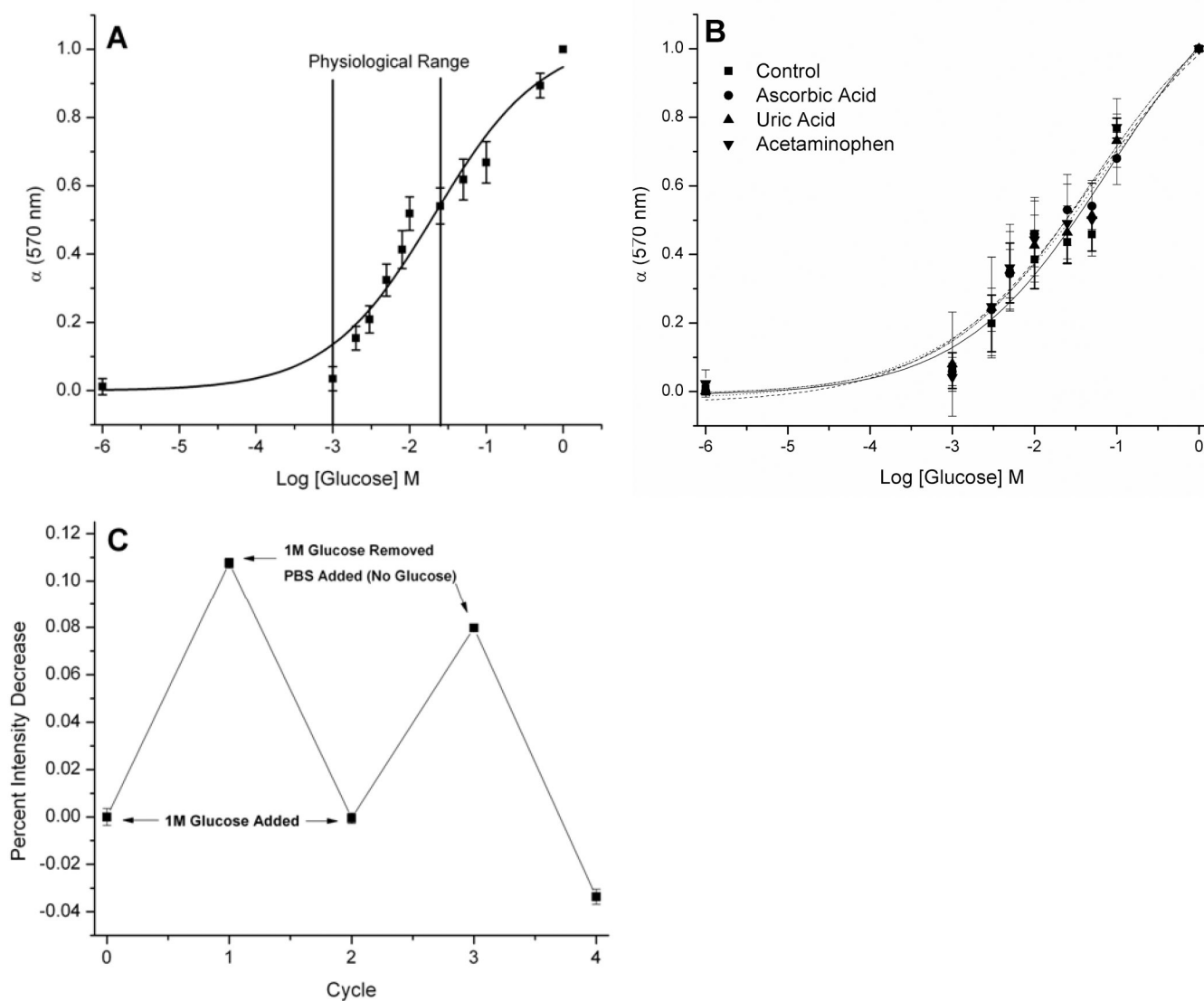
## Acknowledgments

This work was supported by the National Institute of General Medicine of the National Institutes of Health under award number R01 GM084366 and by Internal Research and Development funding from The Charles Stark Draper Laboratory.

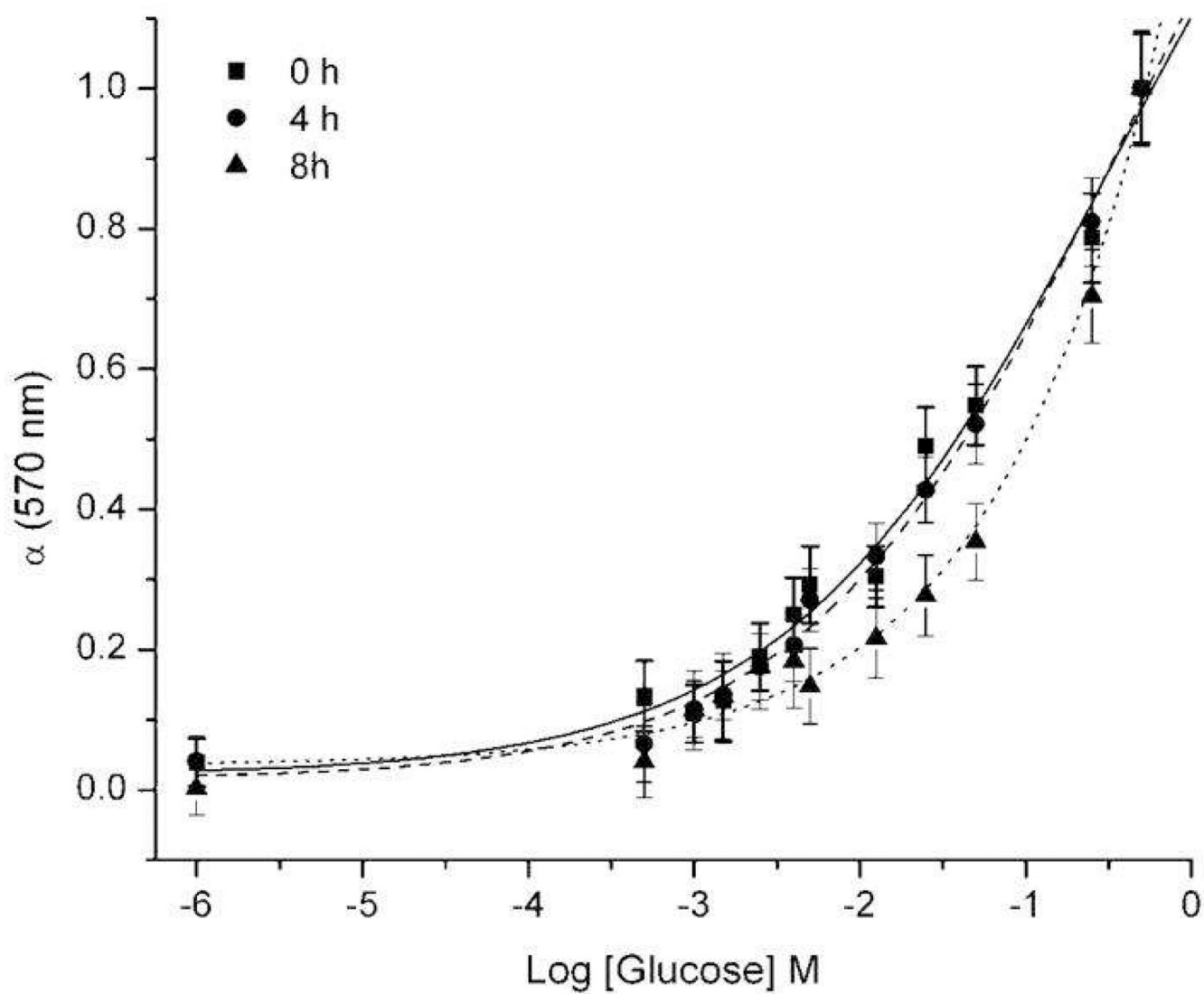
## REFERENCES

1. Brasuel MG, Miller TJ, Kopelman R, Philbert MA. *Analyst* 2003;128:1262–1267. [PubMed: 14667163]
2. Clark H, Barker S, Brasuel MG, Miller M, Monson E, Parus S, Shi Z, Song A, Thorsrud B, Kopelman R, Ade A, Meixner W, Athey B, Hoyer M, Hill D, Lightle R, Philbert MA. *Sens. Actuators* 1998;B: 12–16.
3. Clark HA, Hoyer M, Parus S, Philbert MA, Kopelman R. *Microchimica Acta* 1999;131:121–128.
4. Clark H, Hoyer M, Philbert M, Kopelman R. *Anal. Chem* 1999;71:4831–4836. [PubMed: 10565274]
5. Clark H, Kopelman R, Tjalkens R, Philbert M. *Anal. Chem* 1999;71:4837–4843. [PubMed: 10565275]
6. Brasuel M, Kopelman R, Kasman I, Miller TJ, Philbert MA. *Proc. IEEE* 2002;1:288–292.
7. Dubach JM, Harjes DI, Clark HA. *Nano Lett* 2007;7:1827–1831. [PubMed: 17497824]
8. Xu H, Aylott J, Kopelman R. *Analyst* 2002;127:1471–1477. [PubMed: 12475037]
9. Rosenzweig Z, Kopelman R. *Anal. Chem* 1996;68:1408–1413. [PubMed: 8651500]
10. Singh M, Verma N, Garg AK, Redhu N. *Sens. Actuators, B* 2008;134:345–351.
11. Russell RJ, Pishko MV, Gefrides CC, McShane MJ, Cote GL. *Anal. Chem* 1999;71:3126–3132. [PubMed: 10450158]
12. Dubach JM, Harjes DI, Clark HA. *J. Am. Chem. Soc.* 2007
13. James TD, Sandanayake K, Shinkai S. *Angew. Chem., Int. Ed.* 1996;35:1910–1922.
14. Hall, DG., editor. *Boronic Acids: Preparation and Applications in Organi Synthesis and Medicine.* Wiley-VCH: Weinheim; 2005.
15. Alexeev VL, Sharma AC, Goponenko AV, Das S, Lednev IK, Wilcox CS, Finegold DN, Asher SA. *Anal. Chem* 2003;75:2316–2323. [PubMed: 12918972]
16. Asher SA, Alexeev VL, Goponenko AV, Sharma AC, Lednev IK, Wilcox CS, Finegold DN. *J. Am. Chem. Soc* 2003;125:3322–3329. [PubMed: 12630888]
17. Ben-Moshe M, Alexeev VL, Asher SA. *Anal. Chem* 2006;78:5149–5157. [PubMed: 16841941]
18. Springsteen G, Wang B. *Tetrahedron* 2002;58:5291–5300.
19. Arimori S, Ward CJ, James TD. *Tetrahedron Lett* 2002;43:303–305.

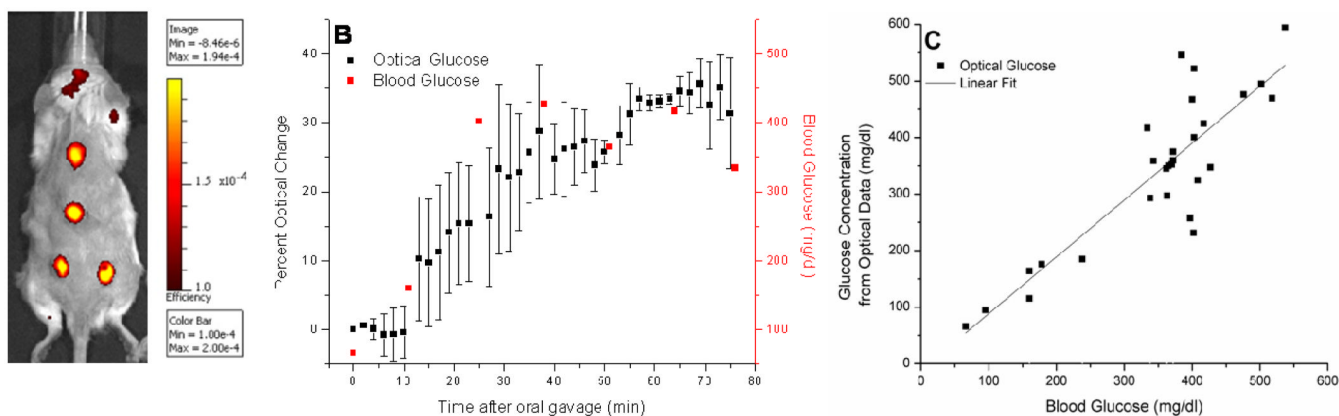
20. Ma WM, Pereira Morais MP, D'Hooge F, van den Elsen JM, Cox JP, James TD, Fossey JS. *Chem. Commun. (Camb)* 2009;532–534. [PubMed: 19283281]
21. McGarraugh G, Sharp C. TheraSense, Inc. 2001
22. Malvern I. Worcestershire. 2005
23. Hrabe de Angelis, M.; Chambon, P.; Brown, SDM. *Standards of Mouse Model Phenotyping*. Wiley-VCH: 2006. Illustrated ed.
24. Tuchin, VV. *Handbook of Optical Sensing of Glucose in Biological Fluids and Tissues*. CRC Press; 2008. Illustrated ed.
25. Patterson S, Smith BD, Taylor RE. *Tetrahedron Lett* 1997;38:6323–6326.
26. Gibney, MJ. *Introduction to Human Nutrition*. Vol. 2. Wiley-Blackwell: 2009. Illustrated ed.
27. Flindt, R. *Amazing Numbers in Biology*. Berlin: Springer-Verlag; 2006. English ed.
28. Sabnis, RW. *Handbook of acid-base indicators*. CRC Press; 2007. Illustrated ed.
29. D, o; H, a; H, editors. *FDA. Services*. 2006. p. 5
30. Hoff J. *Lab Animal* 2000;29:7.
31. Glassberg BY. *Arch. Intern. Med* 1930;46:605–609.
32. Nielsen JK, Djurhuus CB, Gravholt CH, Carus AC, Granild-Jensen J, Orskov H, Christiansen JH. *Diabetes* 2005;54:1635–1639. [PubMed: 15919783]
33. Bolincier J, Ungerstedt U, Arner P. *Diabetologia* 1992;35:1177–1180. [PubMed: 1478372]
34. Schaupt L, Ellmerer M, Brunner GA, Wutte A, Sendlhofer G, Trajanoski Z, Skrabal F, Pieber TR, Wach P. *Am. J. Physiol. Endocrinol. Metab* 1999;276:401–408.



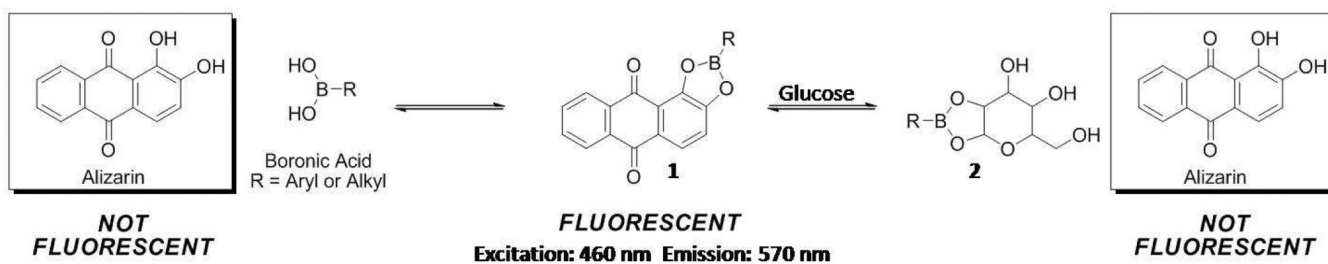
**Figure 1.** Response of optical macrosensor to glucose. (A) Calibration curve and (B) effects of chemical interferents on the calibration. Mean  $\pm$  SD ( $n = 24$ ) for A and mean  $\pm$  SD ( $n_{\text{control}} = 9$ ,  $n_{\text{ascorbic acid}} = 8$ ,  $n_{\text{uric acid}} = 9$ ,  $n_{\text{acetaminophen}} = 8$ ) for B is shown. There was no statistically significant difference in response to these common interferents with  $p > 0.01$  when compared to the control at each concentration. (C) Reversibility of the response to glucose. Percent change refers to the loss of fluorescence intensity exhibited by macrosensor when exposed to 1M glucose in PBS versus control (PBS) ( $n_{\text{control}}=7$  and  $n_{\text{glucose}}=6$ ).



**Figure 2.** Response of optical nanosensors to glucose in PBS. Calibration curve of the nanosensors at 0, 4, and 8 hours. Average of quadruplicate samples from four independent samples.

**Figure 3.**

*In vivo* response of nanosensors to glucose. (A) Image of mouse injected at four locations with glucose-sensitive nanosensors. Image was obtained with an IVIS®-Spectrum imaging system. Excitation and emission wavelengths were 500 nm and 600 nm, respectively. Intensity bar displays the normalized fluorescence efficiency, which represents the fractional ratio of fluorescent emitted photons per incident excitation photon. Residual background fluorescence was attributed to remaining fur. (B) The representative response to oral gavage of the blood glucose (red) and fluorescence of the glucose nanosensors (black). Mean  $\pm$  SD for one mouse is shown. (C) Correlation *in vivo* between optical response of nanosensors and blood measurements. Glucose concentration from optical data vs. blood glucose is shown for all mice ( $n = 4$ ). Error bars are omitted for clarity. A line was fitted to the plot (slope = 1.0,  $R^2 = 0.75$ ).

**Scheme 1.**

Chemical equilibrium of boronate formation between a boronate ester, **1**, and glucose to form a glucose-derived boronate ester, **2**